

LEARNING FROM LIMITED TEMPORAL DATA: DYNAMICALLY SPARSE HISTORICAL FUNCTIONAL LINEAR MODELS WITH APPLICATIONS TO EARTH SCIENCE

BY JOSEPH JANSSEN^{1,a}, SHIZHE MENG^{2,d}, ASAD HARIS^{1,b}, STEFAN SCHRUNNER^{3,e},
JIGUO CAO^{4,7,f}, WILLIAM J. WELCH^{5,g}, NADJA KUNZ^{6,h} AND ALI A. AMELI^{1,c},

¹Department of Earth, Ocean and Atmospheric Sciences, University of British Columbia, ^ajoejanssen@eoas.ubc.ca;
^baharis@eoas.ubc.ca; ^caameli@eoas.ubc.ca

²Department of Mathematics, University of British Columbia, ^dmshizhe@students.cs.ubc.ca

³Department of Data Science, Norwegian University of Life Sciences, ^estefan.schranner@nmbu.no

⁴Department of Statistics and Actuarial Science, Simon Fraser University, ^fjiguo_cao@sfu.ca

⁵Department of Statistics, University of British Columbia, ^gwill@stat.ubc.ca

⁶Norman B Keevil Institute of Mining Engineering, University of British Columbia, ^hnadja.kunz@ubc.ca

⁷Corresponding author: Jiguo Cao, jiguo_cao@sfu.ca

Scientists and statisticians often want to learn about the complex relationships that connect two variables that vary over time. Recent work on sparse functional historical linear models confirms that they are promising for this purpose, but several notable limitations exist. Most importantly, previous works have imposed sparsity on the coefficient function, but have not allowed the sparsity, hence lag, to vary with time. We simplify the framework of sparse functional historical linear models by using a rectangular coefficient structure along with Whittaker smoothing, then relax the previous frameworks by estimating the dynamic time lag from a hierarchical coefficient structure. We motivate our study by aiming to extract the physical rainfall-runoff processes hidden within hydrological data. We show the promise and accuracy of our method using four simulation studies, justified by two real sets of hydrological data.

1. Introduction. In many complex systems, the impact of a cause on some response of interest is distributed across time. Exactly how this impact spreads and changes across time is of great interest to scientists and policy-makers in a wide variety of disciplines. This question not only relates to the magnitude of the effects, but also to exploring how far back in time the cause has a significant impact on the response. If a method for learning this impact function in a data-driven manner existed, one would be able to extract useful knowledge from a variety of time series data sources.

More specifically, this research is motivated by the desire to learn the data generating processes behind hydrological temporal data (Botter, Bertuzzo and Rinaldo, 2010). Learning the different data generating processes across a variety of catchments around the world will allow hydrologists to infer the geological or climatological factors that cause process variation (Schuite et al., 2019). A greater understanding of process variation will enable better predictions in regions where streamflow is not measured. Observational units in hydrology called catchments, filter rainfall and snowmelt into streamflow (Figure 1). This process may seem simple; however, slightly different geologic, climatic, or topographic features may produce vastly different filtering functions (Blöschl et al., 2013). The percent of precipitation that is

Keywords and phrases: Functional data analysis, Hydrology, Precipitation, Rainfall-runoff relationships, Streamflow, Time lag, Whittaker smoothing.

partitioned into streamflow versus water storage versus evaporation can form wildly different ratios, and the time it takes for input water to become streamflow can vary from minutes to years (Jasechko et al., 2016). Figure 1 illustrates these processes. After precipitation falls, it can either transport out of the catchment via evapotranspiration, or it can be transferred into flow. The depth to which water flows or gets stored in/on the ground dictates the length of time between a precipitation event and a rise in streamflow. Overland flow (OF) is transferred into streamflow in a few hours or days. Shallow subsurface flow (SF) is transferred to streamflow in weeks or months, while deep groundwater flow (GF) gets transferred in months or years.

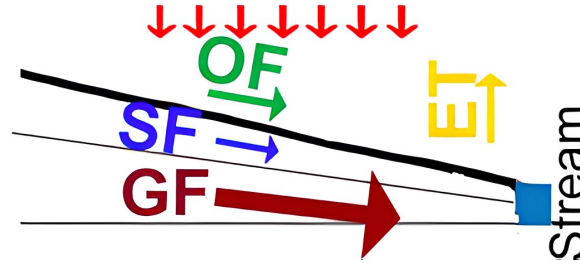


FIG 1. A flow path diagram depicting how precipitation (red arrows) gets partitioned into evapotranspiration (ET, yellow), or different types of flow (green, blue, brown) on a hillslope. Overlandflow (OF, green), shallow subsurface flow (SF, blue) and deep groundwater flow (GF, brown) eventually reach the stream and become streamflow (light blue). The size of each arrow depicts the relative influence of each component in a hypothetical catchment.

Figure 2 displays the daily streamflow and rainfall from the Koksilah River (British Columbia) and the Withlacoochee River (Florida) for the year 1998, illuminating the fact that the complex relationship between rainfall and streamflow not only varies across different catchments, but also across different seasons (Chiu and Bittler, 1969). At the Koksilah River, winter rainfall does not get evaporated (days 1-50 and days 320-365), rather it quickly transfers to streamflow. On the other hand, in summer and early fall (days 100-310), any rainfall that may occur does not seem to result in notable streamflow during these months (top of Figure 2). At the Withlacoochee River, streamflow falls less rapidly during periods of little-to-no rainfall compared to the Koksilah River (e.g., days 1-50 and days 80-120). Evaporation is likely to be large in this catchment, therefore, streamflow may only increase in the event of a large rainfall event as seen on day 50. In the summer and fall (days 150-320), moderate to large rainfall events may not produce streamflow.

Understanding these types of hydrological processes is vitally important for a variety of reasons. For example, the mining sector, which is a significant economic driver in many countries globally, is also highly vulnerable to local hydrology. In Australia, flooding events in the Bowen Basin coal mining region were attributed to billion-dollar production losses for the industry and led to concerns about the impacts of saline mine discharge on surrounding ecosystems (Vink and Robbins, 2012). Mining also alters its surrounding landscape which can impact the water cycle. There are numerous examples of mining regions that have perpetual water quality legacy issues, including selenium pollution and acid rock drainage, which are mobilized due to local hydrology (Kunz, 2020). Improved understanding of hydrological relationships can serve an important role in mitigating such impacts. Likewise, understanding the underlying hydrological structure of a landscape can serve to identify regions that might be more hydrologically vulnerable to major land use changes. For example, knowing that a catchment filters most rainfall slowly through subsurface and deep flow pathways would indicate that the stream is vulnerable to soil and deep rock contamination (Figure 1).

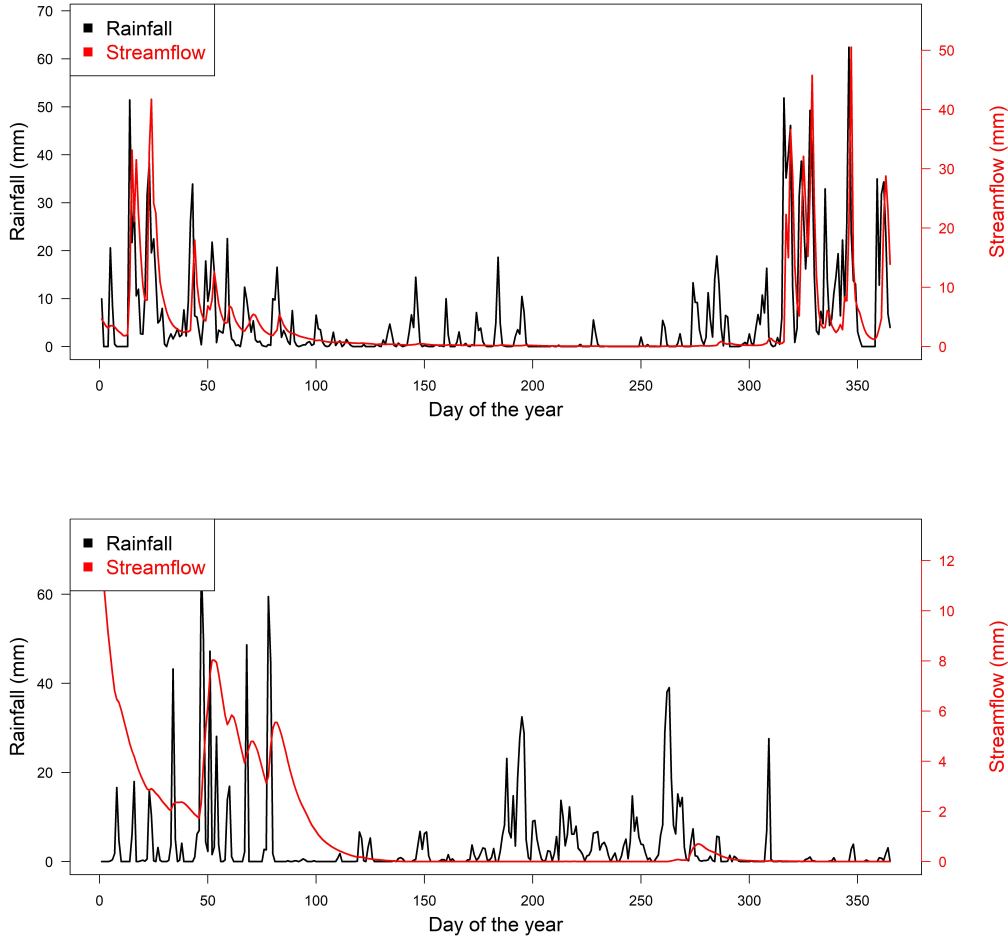


FIG 2. The daily streamflow (red) and rainfall (black) for the Koksilah River (top) and the Withlacoochee River (bottom) for the year 1998.

When predicting streamflow, it is common to assume an arbitrary fixed window of time for which precipitation can affect streamflow, however, this is a severe limitation of previous works (Janssen, Radić and Ameli, 2021), so finding good constant or dynamic time lags is of interest to the hydrological community. Further, learning these parameters at different catchments around the world would allow hydrologists to learn what catchment factors have the biggest influence on the shape of the impact function. Since climate and land use changes will continue to occur, it would be of particular interest to understand where these changes will have outsized impacts on local hydrology. Before advancements in hydrology can be made in this direction, we must first be able to accurately estimate the impact function of precipitation on streamflow.

Xun, Guan and Cao (2022) considered the historical functional linear model,

$$(1) \quad y_i(t) = \int_0^t \beta(s, t) x_i(s) ds + \epsilon_i(t),$$

to study a constant time lag historical effect. Here $y_i(t)$ is the outcome of interest at time t of replicate series i , and $x_i(s)$ is a temporal explanatory variable at the past time s for the same

replicate. The bivariate coefficient function $\beta(s, t)$ represents the effect of the explanatory variable at time s on the outcome at the current time t , where $0 \leq s \leq t$. Note that for the entirety of this work, we ignore the intercept term without loss of generality by removing the seasonal average from $y_i(t)$ and $x_i(t)$. The residual term is denoted by $\epsilon_i(t)$. To estimate $\beta(s, t)$, [Xun, Guan and Cao \(2022\)](#) minimized an objective function containing three terms: (1) a least-squares loss, (2) a nested group bridge penalty term, and (3) a smoothness penalty term. These terms will be further discussed in Section 2, but in summary, the two penalty terms allow the method to infer a sparse and smooth version of the coefficient function, while the least-squares term pushes the optimization towards a solution that fits the data well. More specifically, the group bridge penalty forces some higher lag coefficients of $\beta(s, t)$ to zero, thereby revealing the constant lag δ , after which $\beta(s, t)$ is zero and the covariate has no effect on the response. Sparse estimation of the coefficient function is often of great interest, though it is rarely considered ([Kim, Şentürk and Li, 2011](#)).

This very recent work by [Xun, Guan and Cao \(2022\)](#) builds upon many previous methods including [Malfait and Ramsay \(2003\)](#) who originally developed the functional historical linear model, and [Harezlak et al. \(2007\)](#) who proposed to impose a discrete difference penalty on the coefficients similar to the P-spline framework ([Eilers, Marx and Durbán, 2015](#)). In each of these works, triangular finite elements with tent-like basis functions are considered to model the coefficient function $\beta(s, t)$. The method introduced by [Xun, Guan and Cao \(2022\)](#) is compelling, though it has several notable downsides. First, it is overly complex. Its original formulation is non-convex, and the optimization requires us to iteratively solve LASSO-equivalent problems until convergence. The tent-like basis functions add computational cost, and the number of basis functions used to estimate the coefficient function is therefore usually restricted (about 230 basis functions were used in previous works). However, it is often recommended to increase the resolution by including as many basis functions as computationally feasible, and instead constrain the model by imposing smoothness ([Eilers and Marx, 2021](#)). Moreover, the finite element framework with tent-like basis functions adds few advantages. Second, the triangular finite element framework artificially imposes a constraint on the maximum time lag (i.e., the domain of integration cannot be negative in Equation 1). In the previous works, each year would be treated as a separate replicate, independent of all other replicates, which for our application poses the question of where to start each year, leading further to problems in determining the cause of streamflow at the beginning of each replicate where independence between replicates cannot be assumed. For example, if one were to utilize the previously proposed functional historical linear models to predict streamflow on day one for the Withlacoochee River in Figure 2, only one value of rainfall (0mm) could be used, leading to the impossibility of predicting this year’s peak streamflow. Third, and perhaps most importantly, as mentioned in future work by [Xun, Guan and Cao \(2022\)](#), the previous frameworks do not allow for a time dependent time-lag parameter $\delta(t)$. Other similar methods, with similar issues, can be found in the distributed lag literature ([Almon, 1965](#); [Eisner, 1960](#); [Griliches, 1967](#); [Trivedi and Lee, 1981](#); [Pesando, 1972](#); [Tanner, 1974](#); [Rushworth et al., 2013](#)).

In our motivating problem, streamflow on some day of the year t is a function of $\delta(t)$ days of historical rainfall. Both streamflow and rainfall are measured as daily accumulations in millimeters, so the data is equally spaced. Ideally, we should be able to learn $\delta(t)$ and the function $\beta(s, t)$ that different catchments employ to turn rainfall into streamflow at a daily scale, even in the presence of substantial noise. Given these circumstances which are not only found in hydrology but also across all areas of Earth sciences, [Eilers \(2003\)](#) suggests using the identity matrix as a basis which is equivalent to zero-degree P-splines. This method is referred to as Whittaker smoothing ([Whittaker, 1922](#)), and it vastly simplifies the degree-three tensor product P-splines used by [Rushworth et al. \(2013\)](#) and the tent function finite element

framework employed by [Malfait and Ramsay \(2003\)](#), [Harezlak et al. \(2007\)](#), and [Xun, Guan and Cao \(2022\)](#), while not hurting performance and improving speed ([Eilers, 2003](#); [Eilers, Marx and Durbán, 2015](#); [Eilers and Marx, 2021](#)). This avoids the need to perform costly preprocessing, removes the need to tune the number of splines ([Eilers and Marx, 2021](#)), and removes the need to assume different functional replicates are independent. Further, computation is fast because Whittaker smoothing can lead to extremely sparse matrices ([Eilers and Marx, 2021](#)).

This article has three major contributions. First, to the best of our knowledge, this is the first attempt to estimate a time-dependent time-lag parameter with historical functional linear models. Second, we simplify and increase the flexibility of previous historical functional linear model methods by replacing the tent-like basis functions with the tensor product Whittaker basis such that higher resolution coefficient and time-lag functions can be recovered. Finally, we successfully demonstrate that our method can lead to novel research directions within hydrology by estimating the ground-truth coefficient function $\beta(s, t)$ and time-dependent time-lag parameter $\delta(t)$, which can be used in a variety of future applications to represent the long-term relationship between rainfall and streamflow.

The remainder of this paper is organized as follows. Our method is formally presented in Section 2 along with its theoretical properties and a sketch of its algorithm. In Section 3, we conduct several experiments on real streamflow data and compare the results to expert knowledge. Next, four simulation experiments in Section 4 assess the quality of parameter estimation at different levels of noise. Finally, in Section 5, we summarize the work, explain the limitations of our method and study, and discuss ideas for future work.

2. Method. Let $y_i(t)$ be the observed response at time $t \in 1 \dots T$ for replicate $i \in 1 \dots n$, let $x_i(t)$ be the corresponding covariate, and let D be the total number of considered lags (i.e., $\delta(t) \in [0, D - 1]$), then the functional historical linear model with noise term $\epsilon_i(t)$ is given by Equation 2 and visualized in Figure 3.

$$(2) \quad y_i(t) = \int_0^{D-1} \beta(s, t) x_i(t - s) ds + \epsilon_i(t)$$

As with [Harezlak et al. \(2007\)](#) and [Xun, Guan and Cao \(2022\)](#) we assume without loss of generality that the response and covariate have had their seasonal signals removed such that both functional variables have mean zero for each day of the year. Not only does usage of rainfall and streamflow anomalies instead of the raw signal remove the need for a functional intercept term, it also removes any potential periodic confounding effects present in both signals ([Moges et al., 2022](#)). In our application, $y_i(t)$ is the daily streamflow during the i -th year, and $x_i(t)$ is the daily rainfall. We note that $t - s$ can be negative. When this occurs, we draw from the end of the previous replicate $i - 1$.

Let $\phi_1(s, t), \dots, \phi_K(s, t)$ denote a sequence of K basis functions. Given these basis functions and their corresponding basis coefficients $\mathbf{b} = [b_1, \dots, b_K]^T$, the coefficient function $\beta(s, t)$ can be denoted as

$$(3) \quad \beta(s, t) = \sum_{k=1}^K b_k \phi_k(s, t).$$

Using this basis expansion, we may reformulate Equation 2 as

$$y_i(t) = \int_0^{D-1} \sum_{k=1}^K b_k \phi_k(s, t) x_i(t - s) ds + \epsilon_i(t)$$

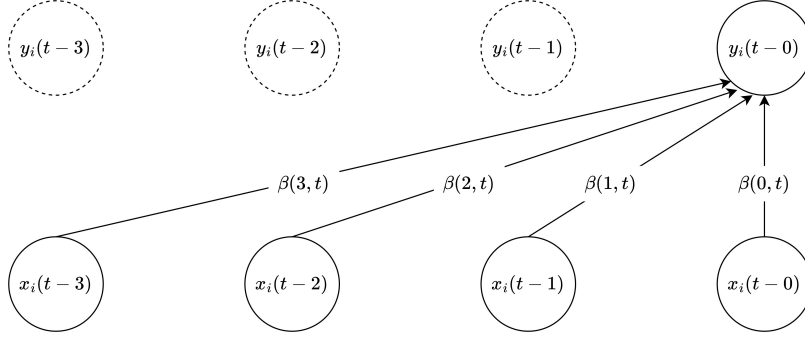


FIG 3. The relationships between the response y and the cause x is shown for $D=4$.

$$\begin{aligned}
 &= \sum_{k=1}^K b_k \int_0^{D-1} \phi_k(s, t) x_i(t-s) ds + \epsilon_i(t) \\
 &= \sum_{k=1}^K b_k z_{ik}(t) + \epsilon_i(t),
 \end{aligned}$$

where

$$z_{ik}(t) = \int_0^{D-1} \phi_k(s, t) x_i(t-s) ds.$$

As stated in the introduction, one of our foremost goals is to infer the dynamic time lag $\delta(t)$ after which the cause has no discernible effect on the response, i.e.,

$$(4) \quad \delta(t) = \max\{s\} \quad \text{subject to } \beta(s, t) \neq 0 \text{ for a given } t.$$

The accuracy in determining $\delta(t)$ is directly related to the resolution of the basis functions that parameterise $\beta(s, t)$. In each of [Harezlak et al. \(2007\)](#), [Rushworth et al. \(2013\)](#), and [Xun, Guan and Cao \(2022\)](#), the time interval is divided into 20 intervals, but when faced with daily data with a yearly period, this gives a resolution for finding $\delta(t)$ of over two weeks. Indeed, $\delta(t)$ may change rapidly, but keeping the functional framework while increasing the number of intervals can be computationally prohibitive.

Under these circumstances, using the Whittaker basis is the most appropriate solution ([Eilers, 2003](#); [Whittaker, 1922](#)). In this work, we parameterize the coefficient function $\beta(s, t)$ with tensor products of Whittaker basis functions $\phi_k(s, t) = w_m(s) \otimes w_\ell(t)$ for $s \in \{1, \dots, D-1\}$ and $t \in \{1, \dots, T\}$. Here $w_m(s)$ and $w_\ell(t)$ denotes the Whittaker basis functions, which are equivalent to zero-degree B-spline basis functions centered at the data points ([Eilers, 2003](#)). If $\phi_1(s, t), \dots, \phi_K(s, t)$ are defined as Whittaker basis functions, the computationally intensive integral term that is found in most historical functional linear model applications reduces to the data points themselves.

Suppose the maximum reasonable lagged influence between $x_i(t)$ and $y_i(t)$ for all t occurs at lag $s = D-1$, then we must estimate $K = DT$ parameters. In general we expect that $nT = N \ll K$, thus the system is often underdetermined. This problem cannot be overcome without some assumptions about the structure of the coefficient function $\beta(s, t)$. Therefore, we stipulate three major assumptions about the structure of $\beta(s, t)$ throughout this work. First, given that we are at the same lag, coefficients at consecutive time points should have similar coefficient values (e.g., $\beta(s, t) \approx \beta(s, t+1)$). Second, given that we

are at the same time point, coefficients at consecutive lags should have similar values (e.g., $\beta(s, t) \approx \beta(s + 1, t)$). Finally, we expect $\beta(s, t)$ to be fairly sparse. Before fitting a model, the extent of the sparsity is unknown, though we expect the sparsity will be in regions with larger lags. Though not explicitly stated, these assumptions also persist throughout the previous works of [Harezlak et al. \(2007\)](#), [Xun, Guan and Cao \(2022\)](#), and [Rushworth et al. \(2013\)](#). We limit the number of assumptions so that our methods are flexible and widely applicable ([Clark, Kavetski and Fenicia, 2011](#)), though we could have further assumed that the coefficient function should be non-negative for our application since additional precipitation cannot reduce streamflow. Instead of adding this constraint, we keep our model flexible in this way and consider this as an additional dimension by which we can evaluate the reliability of our method.

With these three assumptions in mind, we may now impose regularization and sparsity constraints on $\beta(s, t)$ to reduce the possibility of overparameterization ([Gasparrini et al., 2017](#)). With the first assumption, we regularize the squared differences of the coefficient function at consecutive points in time. This can be done with the horizontal first difference penalty matrix (D_H), which was first applied to functional historical linear models in [Harezlak et al. \(2007\)](#) and further used by [Xun, Guan and Cao \(2022\)](#). We further add periodic boundary conditions to D_H in a similar fashion as [Garcia \(2010\)](#), such that $\beta(s, T) \approx \beta(s, 1)$. Likewise, given the second assumption, we may penalize the squared differences between coefficients with the same time but with consecutive lag values by introducing the vertical first difference penalty matrix (D_V). We additionally consider a zero top boundary condition on the vertical penalties since lags past $D - 1$ are assumed to have zero influence. The structure of the coefficients and the penalties are visualized in Figure 4. Further, if we take $D = 2$, $T = 3$, and $K = 6$, then D_V , D_H , and $\beta(s, t)$ are given by:

$$D_V = \begin{bmatrix} -1 & 1 & 0 & 0 & 0 & 0 \\ 0 & 0 & -1 & 1 & 0 & 0 \\ 0 & 0 & 0 & 0 & -1 & 1 \\ 0 & 1 & 0 & 0 & 0 & 0 \\ 0 & 0 & 0 & 1 & 0 & 0 \\ 0 & 0 & 0 & 0 & 0 & 1 \end{bmatrix} \quad D_H = \begin{bmatrix} -1 & 0 & 1 & 0 & 0 & 0 \\ 0 & -1 & 0 & 1 & 0 & 0 \\ 0 & 0 & -1 & 0 & 1 & 0 \\ 0 & 0 & 0 & -1 & 0 & 1 \\ 1 & 0 & 0 & 0 & -1 & 0 \\ 0 & 1 & 0 & 0 & 0 & -1 \end{bmatrix} \quad \beta(s, t) = \begin{bmatrix} \beta(0, 1) \\ \beta(1, 1) \\ \beta(0, 2) \\ \beta(1, 2) \\ \beta(0, 3) \\ \beta(1, 3) \end{bmatrix}.$$

Most previous works that have developed historical functional linear models have imposed sparsity in their model ([Harezlak et al., 2007](#); [Malfait and Ramsay, 2003](#); [Xun, Guan and Cao, 2022](#)), however, they all assume that the lag after which the explanatory feature has no effect on the response is static in time. This assumption is indeed too strong for many applications, especially in Earth science. Instead, we impose sparsity with a more flexible approach via nested group 2-norm thresholding such that a dynamic time lag $\delta(t)$ can be reliably estimated. In statistics, sparsity is usually induced via the lasso or bridge penalties ([Xun, Guan and Cao, 2022](#); [Tibshirani, 1996](#); [Huang, Horowitz and Ma, 2008](#)). The lasso is known to not have the oracle and sign consistency properties, meaning it cannot distinguish which coefficients should be exactly zero according to the data-generating process. This was shown experimentally in the original lasso paper ([Tibshirani, 1996](#)), and it was shown theoretically in [Meinshausen and Yu \(2009\)](#), [Zhao and Yu \(2006\)](#), [Fan and Li \(2001\)](#), and [Leng, Lin and Wahba \(2006\)](#). The oracle and consistency properties of bridge penalties are better than lasso, though they still fail when the number of parameters exceeds the number of observations and when there is extensive multicollinearity ([Huang, Horowitz and Ma, 2008](#)). Both of these troublesome properties are expected in problems surrounding our intended application. As an alternative, [Zhao and Yu \(2006\)](#) suggests using the L0 penalty, though this poses a new problem of non-convexity and NP-hard computational complexity ([Zhao and Yu, 2006](#); [Huo](#)

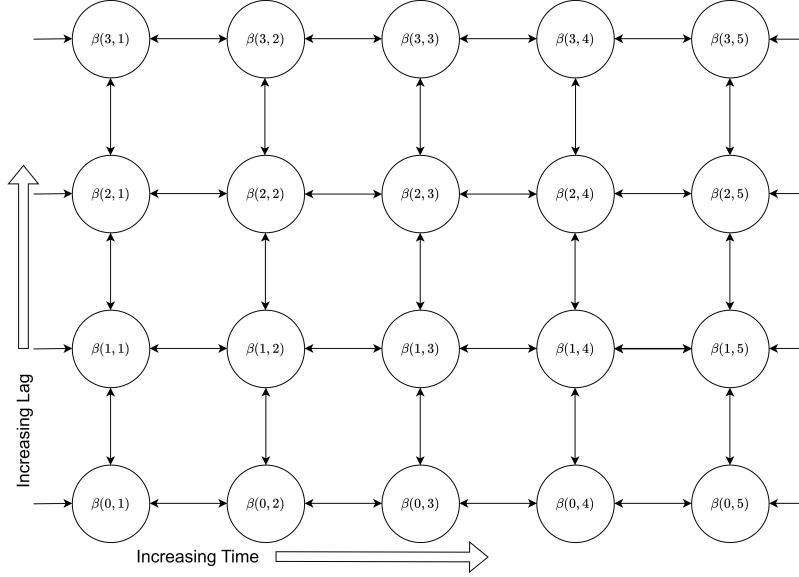


FIG 4. The relationships and general structure of the coefficient function $\beta(s, t)$ are shown for $D = 4$ and $T = 5$, where s increases along the vertical axis, and t increases along the horizontal axis. The lines between nodes indicate that the nodes should have similar values. The partial lines at the sides of the diagram indicate that there is periodic behavior with a period of $T + 1$ (i.e., $\beta(0, 5)$ and $\beta(0, 1)$ are connected). The bottom row of nodes represent the coefficients relating the current time's cause to the current time's response while the next rows represent the coefficients for consecutive time points in the past.

and Ni, 2007). The L0-norm has the oracle property and is selection consistent, meaning it will select the correct features which are non-zero in the ground-truth model with a probability converging to 1 under weaker conditions compared to the lasso (Zhang and Zhang, 2012; Staerk, Kateri and Ntzoufras, 2018; Kim, Kwon and Choi, 2012). Due to the strongly hierarchical nature of our model, optimizing the L0-norm problem changes from $O(2^K)$ to $O(K)$, thus, for our application it is computationally tractable and theoretically preferable for variable selection.

The nested group framework allows us to place each coefficient in a series of groups according to a hierarchical structure (Zhao, Rocha and Yu, 2009). Let $A_{0,t}, A_{1,t}, \dots, A_{D-1,t}$ be a series of groups defined for each time point $t \in 1, \dots, T$. The group $A_{s,t}$ contains the indices of the coefficients corresponding to $\beta(s, t), \dots, \beta(D-1, t)$. Notice that the groups are nested such that $A_{D-1,t} \subset A_{D-2,t} \subset \dots \subset A_{0,t}$. The response Y is defined as a column vector of length $N - (D - 1)$. We then define the sparse matrix $\mathbf{Z} \in \mathbb{R}^{N-(D-1) \times K}$ which has D non-zero entries in each row corresponding to the valid entries of $\beta(s, t)$ given the current time of $y_i(t)$. Here, \mathbf{b} is the vector of $b_k \forall k \in 1, \dots, K$. For example, suppose $n = 2$, $D = 2$, $T = 3$, and $K = 6$, then

$$\mathbf{Y} = \begin{bmatrix} y_1(2) \\ y_1(3) \\ y_2(1) \\ y_2(2) \\ y_2(3) \end{bmatrix} \quad \mathbf{Z} = \begin{bmatrix} z_{1,1}(2) & z_{1,2}(2) & z_{1,3}(2) & z_{1,4}(2) & z_{1,5}(2) & z_{1,6}(2) \\ z_{1,1}(3) & z_{1,2}(3) & z_{1,3}(3) & z_{1,4}(3) & z_{1,5}(3) & z_{1,6}(3) \\ z_{2,1}(1) & z_{2,2}(1) & z_{2,3}(1) & z_{2,4}(1) & z_{2,5}(1) & z_{2,6}(1) \\ z_{2,1}(2) & z_{2,2}(2) & z_{2,3}(2) & z_{2,4}(2) & z_{2,5}(2) & z_{2,6}(2) \\ z_{2,1}(3) & z_{2,2}(3) & z_{2,3}(3) & z_{2,4}(3) & z_{2,5}(3) & z_{2,6}(3) \end{bmatrix} \quad \mathbf{b} = \begin{bmatrix} b_1 \\ b_2 \\ b_3 \\ b_4 \\ b_5 \\ b_6 \end{bmatrix}.$$

Our method first estimates a smooth coefficient function via:

$$(5) \quad \min_{\mathbf{b}} \|\mathbf{Y} - \mathbf{Z}\mathbf{b}\|_2^2 + w_h \|D_H \mathbf{b}\|_2^2 + w_v \|D_V \mathbf{b}\|_2^2$$

Then, the group 2-norms are computed and a model is refit using coefficients with corresponding group norms greater than some threshold q (Equation 6). A clear and detailed description of our algorithm is provided in Algorithm 1.

$$(6) \quad \min_{\mathbf{b}} \|\mathbf{Y} - \mathbf{Z}\mathbf{b}\|_2^2 + w_h \|D_H \mathbf{b}\|_2^2 + w_v \|D_V \mathbf{b}\|_2^2 \text{ s.t. } \mathbf{b}_{A_{s,t}} = 0 \text{ when } \|\mathbf{b}_{A_{s,t}}\|_2^2 < q$$

Algorithm 1:

-
- Require:** One response time series $Y = [y_1, \dots, y_N]$ and one explanatory time series $X = [x_1, \dots, x_N]$.
- 1: Find optimal weights w_h, w_v such that some objective function is maximized on a validation set.
 - 2: Find optimal \mathbf{b} using the optimal weights w_h and w_v and the least squares criterion in Equation 5.
 - 3: Compute the group norms $\|\mathbf{b}_{A_{s,t}}\|_2^2$ for all (s, t) .
 - 4: Find optimal sparsity threshold q .
 - 5: Given q , recompute the optimal smoothing weights, w_h and w_v , and refit the model using all data.
 - 6: **return** $\beta(s, t)$ and $\delta(t)$
-

3. Hydrology Data Application. Since this paper is motivated by problems in hydrology, we use hydrology data for both our simulated and real data experiments. We select two diverse catchments to show the versatility of our method. The first catchment we explore is the Koksilah River which is located in Cowichan, British Columbia, Canada. The area of this catchment is 236km² with an average elevation of 461 meters. 11% of precipitation falls as snow and it is an extremely wet catchment with an aridity index of just 0.37. The second catchment we explore is the Withlacoochee River which is located in Dade City, Florida, United States. The area of the catchment is 650km², and it is low lying with an average elevation of only 42 meters above sea level. It does not experience any snow and it is a fairly dry catchment with an aridity index of 1.07. Clearly these two catchments hold significantly different attributes, making them distinctly interesting case studies (Janssen, Radić and Ameli, 2021). To obtain rainfall for both these areas, we use EMDNA (Tang et al., 2021), a high-quality climate dataset that has complete daily precipitation and temperature values for 1979-2018 at 10km grid squares across North America. From this data, daily rainfall values are generated for the Koksilah and Withlacoochee rivers by averaging precipitation and temperature values across the catchments, then using a temperature threshold of 0 degrees Celsius, we separate rainfall from snowfall (Figure 5). Leap days are removed, leaving us with $365 * 40 = 14,600$ observations. We decided that the maximum reasonable lag should be $D = 150$ since, no matter the location, all precipitation in rain-dominated catchments should drain, become captured by deep groundwater systems, or be evaporated from the catchment within 150 days (5 months) (Jasechko et al., 2016), leaving a total of $365 * 150 = 54,750$ parameters to be estimated within $\beta(s, t)$. The choice of maximum lag also alters the total number of available observations since to predict the response we require the previous 150 days of explanatory data. Therefore, the final number of observations is 14,451.

Hyperparameters w_h and w_v are optimized with Bayesian optimization given a Gaussian process prior using the GPfit R package (MacDonald, Ranjan and Chipman, 2015). We start with 30 uniformly random initial points, then continue by choosing the next point by maximizing the expected increase in validation set R^2 for 35 iterations. After experimenting on

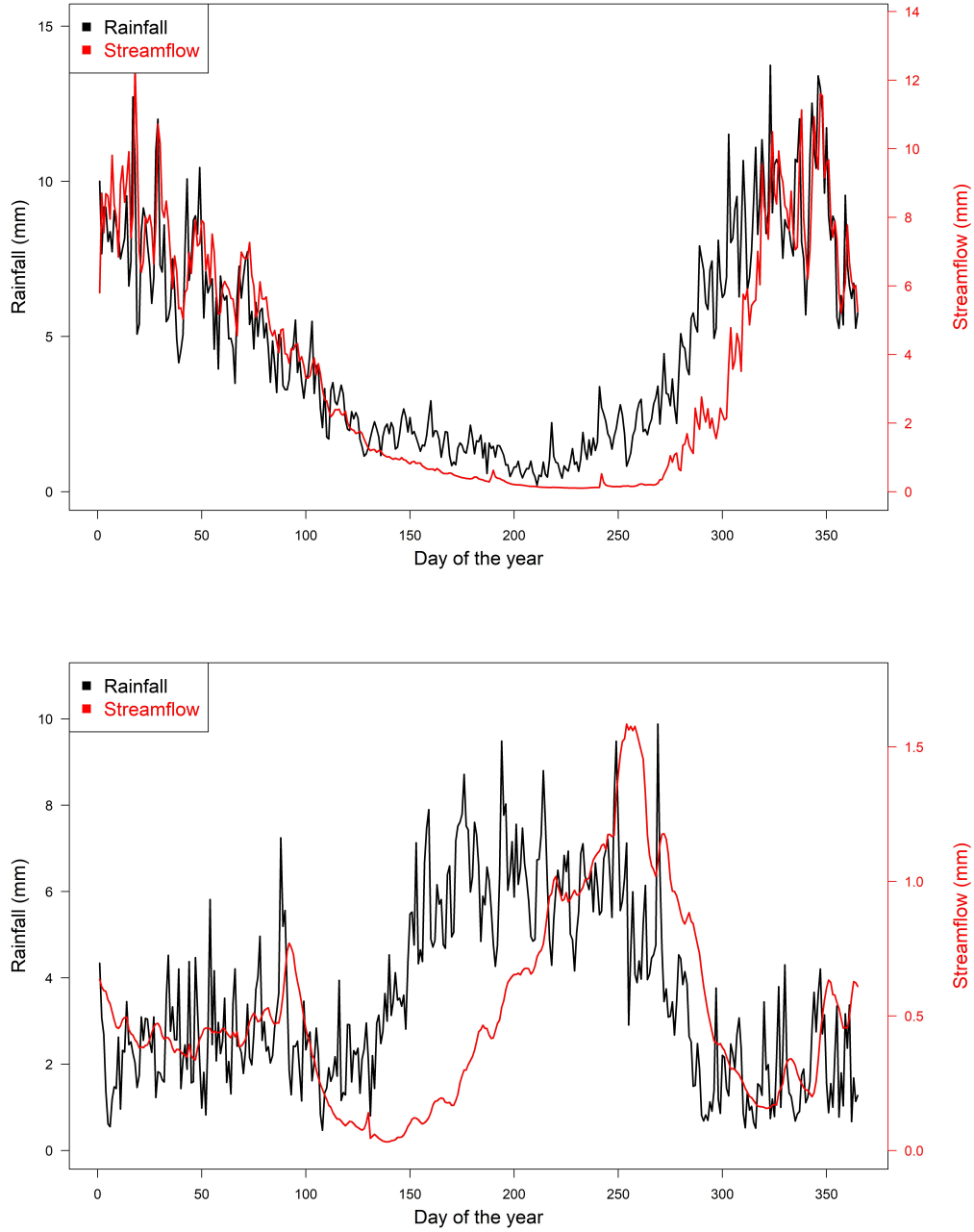


FIG 5. The average daily streamflow (red) and rainfall (black) for the Koksilah River (top) and the Withlacoochee River (bottom) for 1979-2018.

several catchments, we noticed that the optimal w_h is often much larger than the optimal w_v , thus we set our search range as $e^{[10,20]}$ for w_h and $e^{[-5,15]}$ for w_v .

Choosing the optimal threshold q is often the most difficult step in Algorithm 1. We do not specifically define how this should be done in the methods section as how to choose the optimal q is still an open question, therefore we leave it up to the user and their goals. If the goal is feature selection, where removing a few important features is not as critical as only

selecting features which are surely important, greater sparsity may be desired. If instead, a lag should only be removed if it is surely unimportant, such as in sure independence screening (Fan and Lv, 2008), future users may desire less sparsity. We aim to satisfy both goals with no specific preference. In the process of our experiments, we tried several methods. Naturally, statisticians and data scientists are drawn towards choosing a q that maximizes validation set R^2 . During testing, this method seemed to give high test set R^2 scores, however, the final coefficient function had small values fluctuating around zero and the simulation results were poor, indicating too little sparsity. The phenomena was also found in Rushworth et al. (2013) who observed optimizing the AIC leads to too little smoothness, pushing the authors to use the AIC-optimal smoothness parameter as a lower bound and artificially increasing this value. The authors believed this point was important enough to include it as a paramount component of future work. These results highlight the diverging goals of prediction and inference (Arlot and Celisse, 2010). A popular alternative method to this is choosing the "knee point" in the plot of q versus the whole dataset R^2 (Satopaa et al., 2011). This method is popular for unsupervised learning such as clustering analysis, though for our purposes, it leads to too much sparsity. Instead of occurring at the middle of the knee, the ground-truth sparsity threshold seemed to often occur at the beginning of the knee, i.e., "knee-onset" (Fermín-Cueto et al., 2020). One promising way to automatically find the "knee-onset" is maximizing Menger curvature between the first, last, and current point (Satopaa et al., 2011), though we found that this method was too sensitive to noise. In all experiments below, we find the "knee-onset" by choosing the first of two knees as outlined in Satopaa et al. (2011) and Fermín-Cueto et al. (2020). All experiments were run in R version 4.2.1.

3.1. Analysis of hydrology data. To obtain real response variable data that pairs with our real rainfall data, daily streamflow data from the Koksilah River was gathered from the HYDAT database (Albers, 2017), and daily streamflow data from the Withlacoochee River was taken from CAMELS (Addor et al., 2017). The average daily streamflow for both rivers is visualized in Figure 5. After performing initial data exploration and methodological experimentation, we decided to transform streamflow Q via $\log(Q + 1)$, since this transform improved predictive performance and removed patterns and non-Gaussianity from the residual plots. The estimates of our hyperparameters w_h and w_v are obtained after splitting the data with 80% of the data for training and 20% of the data for validation. The final estimates of $\beta(s, t)$, $\delta(t)$, and the whole dataset R^2 are then obtained by training on all available data. We also evaluate the predictive performance of our model with a test set. To compute test set R^2 values, we split the data with 60% for training, 20% for optimizing the hyperparameters w_h and w_v , and 20% for testing. We present our results for both rivers below.

The estimated $\hat{\beta}(s, t)$ for the Koksilah River after training on the entire dataset is shown in Figure 6. The whole dataset R^2 was 0.74 when trained on all data. On the test set, the R^2 was 0.81. In winter, rainfall frequency and magnitude peaks after a rapid ramp up from September to October to November (days 260-320), therefore, by December (day 335), the soil in the catchment is full of water and groundwater is fully connected (Figure 5). When this happens, any additional rain either immediately transmits to flood waters heading towards the stream, or the additional rainfall quickly pushes the water already in the soil towards the stream. Further, this behavior can be seen in Figure 5, where December, January, and February (days 330-70) streamflow correlates strongly with rain falling the previous day. Therefore, observing a $\delta(t)$ of around 3 days from day 350-60 empirically confirms and supports existing expert knowledge. Two distinct peaks of maximum lag appear in summer and fall in Figure 6. The peak in summer at around day 190, with a $\delta(t)$ of about 18 days displays a long term recession behavior in the catchment. Starting in March, this catchment appears to enter a drying phase where evapotranspiration and runoff exceed water input (Figure 5). During the

drying phase, rainfall further back in the past begins to make a larger difference on current streamflow, since the relative amount of dryness is a significant driver for streamflow production. During August (around day 230), the soil is completely dry and temperatures are high, therefore most rainfall contributes to soil wetness and evaporation instead of streamflow. Starting in mid-September (day 260), the Koksilah River catchment enters a rapid wetting phase as rainfall quickly becomes more frequent. Rainfall occurring up to around 40 days in the past begins to have a significant impact on streamflow, since during this time if the previous days were dry any additional precipitation will contribute to soil wetness, but if previous days were wet, additional precipitation will contribute to streamflow. The wetting phase ends in December (about day 350) when the soil becomes fully saturated regardless of the between-year variations of precipitation in the wettest month, November.

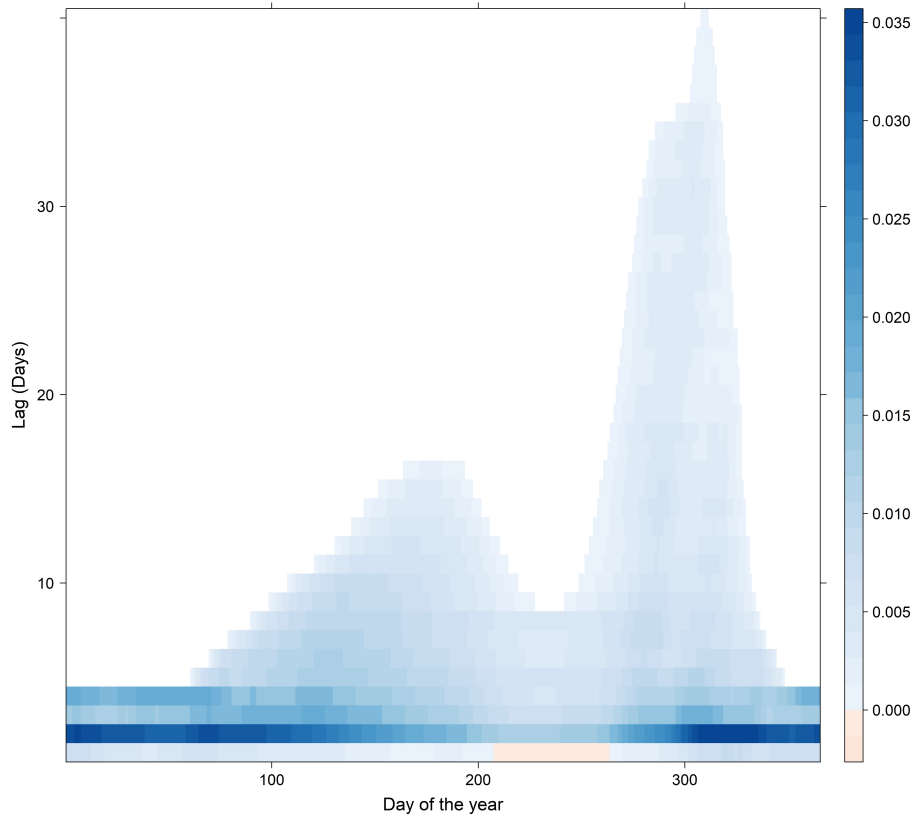


FIG 6. The estimated function $\hat{\beta}(s, t)$ for each lag s and time t for the Koksilah River located in British Columbia from the whole data period (1979-2018).

For the second catchment, the Withlachoochee River in Florida, the R^2 was 0.58 on the test dataset. The final whole dataset R^2 for this catchment when trained on the entire dataset was 0.54 (Figure 7). It is not surprising that the whole-dataset R^2 is often lower than the test set R^2 . This just indicates that the training set is extremely hard to predict, perhaps due to high or more frequent extremes which are notoriously hard to predict, especially with only a linear model. The test set R^2 results for both catchments are similar to those seen from LSTMs

which are much more complex and much less interpretable (Hoedt et al., 2021; Anderson and Radić, 2022).

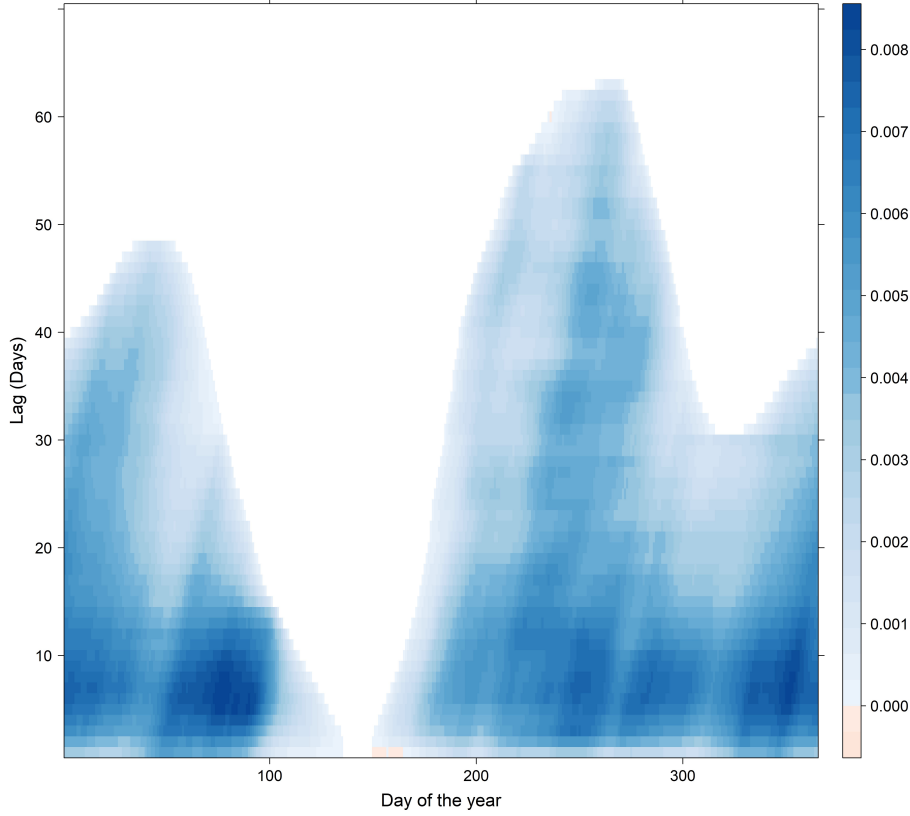


FIG 7. The estimated function $\hat{\beta}(s, t)$ for each lag s and time t for the Withlachoochee River, located in Florida, after training on the whole dataset (1979-2018).

Though the Withlachoochee River results presented in Figure 7 look very different compared to the results from the Koksilah River (Figure 6), the results can be interpreted in a similar fashion. We first note that this catchment never reaches a fully saturated phase where rainfall has a huge impact on streamflow in a short period of time. This is reasonable since this is a dry catchment with an aridity index of greater than one, meaning that the potential for evaporation is greater than total precipitation. Starting in May (days 130-175), the catchment enters a dry phase. By this time of the year, the catchment has experienced about 6 months of relatively dry weather and temperatures have begun to rise (Figure 5), therefore in May, any rainfall that occurs gets evaporated or contributes to soil moisture. By mid to late June (about day 180), a consistent amount of rainfall usually falls, outpacing evaporation and streamflow (Figure 5), thus the catchment soils become wet enough to produce streamflow. Before the catchment can become fully saturated, in September (day 260), rainfall falls below evaporation and streamflow, leading to larger lags becoming significant and a drying phase from October to the next year.

Both real-world studies lead to interesting and meaningful results with good R^2 scores on the test set. In both cases, wetting, wet, drying, and dry periods could be delineated. Further,

even though the positivity of the coefficient function was not imposed as a constraint for our models, in both cases, the model correctly identified that there is a strong positive relationship between rainfall and streamflow. A few places with negative coefficients appeared, but the negative locations were highly limited and the magnitude of the negative coefficients were extremely small. This is a further indication that our method is reliable and can correctly identify dominant processes.

4. Simulation Studies. The aim of our simulation study is to quantify and understand our ability to estimate $\beta(s, t)$ and $\delta(t)$ in a variety of noisy environments.

4.1. Evaluation criteria. Both [Malfait and Ramsay \(2003\)](#) and [Harezlak et al. \(2007\)](#) were interested in model predictions, so in line with their goals, they assessed their methods in simulation studies by computing R^2 values between the predicted and ground-truth response values. In contrast to this, the goal of [Xun, Guan and Cao \(2022\)](#) was statistical inference, so they compared methods by their accuracy in estimating $\beta(s, t)$ and δ . More specifically, they compute the root mean squared error of δ , the percent bias of δ , and the mean integrated squared error of $\beta(s, t)$. The percent bias of δ does not fully capture the accuracy of δ estimates when δ varies over time, and the other metrics are less interpretable compared to the R^2 metric used by [Malfait and Ramsay \(2003\)](#) and [Harezlak et al. \(2007\)](#), thus we introduce three evaluation criteria for our simulation studies. The first criterion, β - R^2 , aims to evaluate the accuracy in estimating the true coefficient function in an interpretable fashion:

$$(7) \quad R^2(\beta, \hat{\beta}) = 1 - \frac{\int \int \{\beta(s, t) - \hat{\beta}(s, t)\}^2 ds dt}{\int \int \{\beta(s, t) - \bar{\beta}\}^2 ds dt}$$

The second criterion, $\delta(t)$ -bias, evaluates the bias appearing in our estimates of $\delta(t)$. We compute this criterion as the average of $\hat{\delta}(t)$ across time minus the average of $\delta(t)$ across time. Our third criterion, $\delta(t)$ -correlation evaluates how well we can estimate the inter-period variability in $\delta(t)$ across time. This metric is simply calculated as the correlation between the ground-truth $\delta(t)$ and the estimated $\hat{\delta}(t)$. Ideally, we would want β - R^2 and $\delta(t)$ -correlation to be close to one, while $\delta(t)$ -bias is close to zero.

4.2. Simulation scenarios. In this section, we run four simulation studies that aim to quantify our method's ability to estimate $\beta(s, t)$ and $\delta(t)$ in noisy environments. We use the same real rainfall data used in the previous section to form the covariate matrix \mathbf{Z} , then we define four scenarios with different values for $\beta(s, t)$, $\delta(t)$, and noise levels, such that known ground-truth values for the response $y_i(t)$ can be simulated. Streamflow is notoriously difficult to predict. Depending on the location of the catchment and its dynamics, even when using powerful black-box methods such as long short-term memory neural networks (LSTMs) ([Hochreiter and Schmidhuber, 1997](#)), combined with more predictor variables, the test set R^2 can range all the way from zero to one ([Ayzel and Heistermann, 2021](#); [Hoedt et al., 2021](#); [Kratzert et al., 2018](#)). In future scenarios for which our method may be applied, we hypothesize that inferences from models with $R^2 < 0.4$ will be difficult. Further, from previous works we know that interpretable models with $R^2 > 0.8$ will be rare in hydrology. Thus, we simulate the response vector with additional noise such that if we calculate the true response $y_{\text{true}}(t)$ from the ground-truth $\beta(s, t)$ we would produce $R^2(y, y_{\text{true}}) = 0.8$ or $R^2(y, y_{\text{true}}) = 0.4$, where $R^2(y, y_{\text{true}})$ is defined in Equation 8, $y(t)$ is the simulated data after adding noise to $y_{\text{true}}(t)$, and \bar{y} is the average of $y(t)$ over t .

$$(8) \quad R^2(y, y_{\text{true}}) = 1 - \frac{\int \{y(t) - y_{\text{true}}(t)\}^2 dt}{\int \{y(t) - \bar{y}\}^2 dt}$$

The calculated value of the variance of the added noise for each simulated scenario is displayed in Table 1.

The four scenarios revolve around the results obtained in the real hydrology study in Section 3.1. The results from each river were quite different, thus we take these results from Figures 6 and 7 and set them as our ground-truth scenarios. Taking these $\beta(s, t)$ values along with our matrix of rainfall values allows us to compute ground-truth response values. With two different noise levels, there are four simulation scenarios. For each scenario, we repeat the simulation 100 times such that stable results and uncertainty levels can be obtained. Each simulation iteration takes less than 10 minutes on an Intel i9-9980HK 2.4 GHz processor with 32 GB of RAM, so our methods are computationally feasible for any modern hardware setup.

4.3. *Simulation results.* Table 1 shows that the introduced method is quite promising and robust. We consistently observe that regardless of location, the data with less noise allowed for more accurate and stable inferences of $\beta(s, t)$, however, the differences are surprisingly small, especially for the Withlacoochee River. For both rivers, the noise level seemed to make little difference in the bias of $\delta(t)$ estimates, where both locations saw slight increases in bias magnitude as we decreased the noise. This suggests that our method for choosing the threshold q is not optimal. For the Withlacoochee River, the estimates for $\beta(s, t)$ are consistently accurate with $R^2 = 0.94$ for the high noise scenario and $R^2 = 0.95$ for the low noise scenario. For both noise scenarios, the bias was about -6 days while the $\delta(t)$ correlation was about 0.99. The average results displayed in Table 1 as well as the individual simulation runs consistently resulted in negative $\delta(t)$ -biases, revealing systematic errors. This indicates that on average $\delta(t) > \hat{\delta}(t)$, meaning that the estimated coefficient function is often too sparse and the chosen q should decrease.

TABLE 1

Summary of the simulation study results. The average (standard deviation) across the 100 replications is shown for each of the evaluation criteria defined in Section 4.1.

Location	$R^2(y, y_{\text{true}})$	Noise variance	β - R^2	$\delta(t)$ -bias	$\delta(t)$ -corr
Koksilah River	0.4	0.244	0.940 (0.021)	-0.971 (0.904)	0.859 (0.094)
Koksilah River	0.8	0.041	0.972 (0.006)	-2.16 (0.598)	0.905 (0.049)
Withlacoochee River	0.4	0.100	0.938 (0.010)	-5.559 (0.837)	0.986 (0.004)
Withlacoochee River	0.8	0.017	0.950 (0.005)	-6.478 (0.398)	0.986 (0.002)

5. Discussion and Conclusions. In this work, we build off the iterations of the functional historical linear model introduced by Malfait and Ramsay (2003), Harezlak et al. (2007), Rushworth et al. (2013), and Xun, Guan and Cao (2022). We greatly simplify their formulations while allowing for dynamic sparsity and high resolution estimates of the coefficient function using the Whittaker basis. In Section 2, we illustrate our algorithm with several diagrams and introduce the three minor assumptions we make to reduce the highly overparameterized problem to one that is tractable. We only assume horizontal smoothness, vertical smoothness, and that sparsity is concentrated at larger lags to keep our methods flexible and applicable to a wide variety of applications outside of our main hydrologically-centered goal. Throughout the work, we are strongly driven by the goal of accurately estimating rainfall-runoff relationships. After gathering rainfall and streamflow data from Vancouver Island and Florida, we estimated the coefficient functions that transfer rainfall to streamflow at both locations and compared our conclusions with expert knowledge. We found that the functions

have a perfect hydrologically-significant interpretation where catchments go through four distinct phases: (1) wetting, (2) wet, (3) drying, (4) dry. Because the Koksilah River (Vancouver Island) has high seasonal variability in temperature and rainfall, the four phases can be distinctly parsed. On the other hand, we found that the Withlachoochee River (Florida) is an extremely dry catchment, therefore it never enters the wet phase, but all other phases can be inferred. Indeed, none of these inferences could have been made without the methodological improvements pertaining to the dynamic sparsity. Finally, in an extensive simulation study, we found that our simple methodology can successfully recover the ground-truth coefficient function $\beta(s, t)$ as well as the dynamic time lag $\delta(t)$ with high accuracy. Though the accuracy for which we can recover the coefficient function and time-lag clearly depend on the level of noise, we found that even when the R^2 is less than or equal to 0.4, accurate conclusions can be made from our inferences.

Several shortcomings of our methods and experiments can be identified. First, our methods are currently limited to bivariate analysis, though Algorithm 1 could easily be extended to include multiple explanatory features. Second, though our algorithm can potentially include multiple features, these additional features may not follow our sparsity and smoothness assumptions. For example, if we included snowfall as a predictor of streamflow in a snow-rich catchment we may expect snowfall to take days or weeks or even months to melt and begin to contribute to streamflow. This would contradict our sparsity assumption since very low and very high lags would be expected to have zero coefficients. Third, the way in which we choose sparsity is fairly arbitrary. Selecting the onset of nonlinearity can be justified by the same theory as the adjusted- R^2 , since the expected decrease in R^2 will be linear if we are removing irrelevant variables, however finding the onset of nonlinearity in an automatic fashion is still an active area of research. Finally, we assume throughout the work that the behavior of the catchment does not change across different years. Although our method does not capture year-to-year relationship variability, our method can be used to extract multiple coefficient functions before and after some known change. For example, one could estimate the rainfall-runoff relationship before and after a large change in land use or before and after a period of severe climate change. Focusing now on the limitations of our experiments, we note that our experiments are only limited to a specific application in hydrology, though we hypothesize that our methods can work well in other domains. Further, our simulation study is limited since we provided ground-truths that we know can be reached from the algorithm. This limitation points back to the second methodological limitation since our method may only be able to recover certain types of coefficient functions. If we instead ran a simulation study with a non-smooth ground-truth, the simulation results would likely be worse.

In future work, one could solve one or more of the above shortcomings. Perhaps the flexibility of our methods could also be improved by adding adaptive smoothness in a similar fashion as the adaptive lasso, since different days or lags could have different smoothness (Zou, 2006; Centofanti et al., 2022; Yang and Hong, 2017; Yang et al., 2021). Alternatively, extending these methods to spatial analysis could be interesting. With smooth spatial attribution, one could understand how impactful a specific grid cell of a cause is on the response. Further, with sparsity, one could delineate the spatial area that is impactful on the response versus the areas which have no significant impact on the response. Our current work takes the perspective of penalized least squares and sparsity thresholding, but another interesting perspective leading to different methods could come from a causal inference and conditional independence framework. For example, finding the correct sparsity using partial correlation or transfer entropy may be possible (Murari et al., 2018; Moges et al., 2022), though the high dimensional and low sample size environment makes this non-trivial. We hope our methods can serve as a reliable tool for learning from time series data across multiple areas of science or serve as an inspiration for further methodological development. This area of research is certainly rich with potential scientific discoveries.

Funding. This research was funded by the Collaborative Research Team Project of Canadian Statistical Sciences Institute (CANSSI) awarded to Ali A. Ameli, William J. Welch, and Jiguo Cao. Joseph Janssen was supported by Natural Sciences and Engineering Research Council of Canada (NSERC) PhD Scholarship. Asad Haris was supported by UBC's Data Science Institute Postdoctoral funding. Jiguo Cao's research was partially supported by the NSERC Discovery grant (RGPIN-2018-06008). Stefan Schrunner gratefully acknowledges the financial support from internal funding scheme at Norwegian University of Life Sciences (project number 1211130114), which financed the international stay at the University of British Columbia, Canada.

SUPPLEMENTARY MATERIAL

Data and Code. We provide the R code, data, and results for the real data analysis and simulation studies in the supplementary material.

REFERENCES

- ADDOR, N., NEWMAN, A. J., MIZUKAMI, N. and CLARK, M. P. (2017). The CAMELS data set: catchment attributes and meteorology for large-sample studies. *Hydrology and Earth System Sciences* **21** 5293–5313.
- ALBERS, S. (2017). tidyhydat: Extract and Tidy Canadian Hydrometric Data. *The Journal of Open Source Software* **2**. <https://doi.org/10.21105/joss.00511>
- ALMON, S. (1965). The distributed lag between capital appropriations and expenditures. *Econometrica: Journal of the Econometric Society* 178–196.
- ANDERSON, S. and RADIĆ, V. (2022). Evaluation and interpretation of convolutional long short-term memory networks for regional hydrological modelling. *Hydrology and Earth System Sciences* **26** 795–825.
- ARLOT, S. and CELISSE, A. (2010). A survey of cross-validation procedures for model selection.
- AYZEL, G. and HEISTERMANN, M. (2021). The effect of calibration data length on the performance of a conceptual hydrological model versus LSTM and GRU: A case study for six basins from the CAMELS dataset. *Computers & Geosciences* **149** 104708.
- BLÖSCHL, G., BLOESCHL, G., SIVAPALAN, M., WAGENER, T., SAVENIJE, H. and VIGLIONE, A. (2013). *Runoff prediction in ungauged basins: synthesis across processes, places and scales*. Cambridge University Press.
- BOTTER, G., BERTUZZO, E. and RINALDO, A. (2010). Transport in the hydrologic response: Travel time distributions, soil moisture dynamics, and the old water paradox. *Water Resources Research* **46**.
- CENTOFANTI, F., LEPORE, A., MENAFOGLIO, A., PALUMBO, B. and VANTINI, S. (2022). Adaptive smoothing spline estimator for the function-on-function linear regression model. *Computational Statistics* 1–26.
- CHIU, C.-L. and BITTLER, R. P. (1969). Linear time-varying model of rainfall-runoff relation. *Water Resources Research* **5** 426–437.
- CLARK, M. P., KAVETSKI, D. and FENICIA, F. (2011). Pursuing the method of multiple working hypotheses for hydrological modeling. *Water Resources Research* **47**.
- EILERS, P. H. (2003). A perfect smoother. *Analytical chemistry* **75** 3631–3636.
- EILERS, P. H., MARX, B. D. and DURBÁN, M. (2015). Twenty years of P-splines. *SORT: statistics and operations research transactions* **39** 0149–186.
- EILERS, P. H. and MARX, B. D. (2021). *Practical smoothing: The joys of P-splines*. Cambridge University Press.
- EISNER, R. (1960). A distributed lag investment function. *Econometrica, Journal of the Econometric Society* 1–29.
- FAN, J. and LI, R. (2001). Variable selection via nonconcave penalized likelihood and its oracle properties. *Journal of the American statistical Association* **96** 1348–1360.
- FAN, J. and LV, J. (2008). Sure independence screening for ultrahigh dimensional feature space. *Journal of the Royal Statistical Society: Series B (Statistical Methodology)* **70** 849–911.
- FERMÍN-CUETO, P., MCTURK, E., ALLERHAND, M., MEDINA-LOPEZ, E., ANJOS, M. F., SYLVESTER, J. and DOS REIS, G. (2020). Identification and machine learning prediction of knee-point and knee-onset in capacity degradation curves of lithium-ion cells. *Energy and AI* **1** 100006.
- GARCIA, D. (2010). Robust smoothing of gridded data in one and higher dimensions with missing values. *Computational statistics & data analysis* **54** 1167–1178.
- GASPARRINI, A., SCHEIPL, F., ARMSTRONG, B. and KENWARD, M. G. (2017). A penalized framework for distributed lag non-linear models. *Biometrics* **73** 938–948.

- GRILICHES, Z. (1967). Distributed lags: A survey. *Econometrica: journal of the Econometric Society* 16–49.
- HAREZLAK, J., COULL, B. A., LAIRD, N. M., MAGARI, S. R. and CHRISTIANI, D. C. (2007). Penalized solutions to functional regression problems. *Computational statistics & data analysis* **51** 4911–4925.
- HOCHREITER, S. and SCHMIDHUBER, J. (1997). Long short-term memory. *Neural computation* **9** 1735–1780.
- HOEDT, P.-J., KRATZERT, F., KLOTZ, D., HALMICH, C., HOLZLEITNER, M., NEARING, G. S., HOCHREITER, S. and KLAMBAUER, G. (2021). Mc-lstm: Mass-conserving lstm. In *International Conference on Machine Learning* 4275–4286. PMLR.
- HUANG, J., HOROWITZ, J. L. and MA, S. (2008). Asymptotic properties of bridge estimators in sparse high-dimensional regression models. *The Annals of Statistics* **36** 587–613.
- HUO, X. and NI, X. (2007). When do stepwise algorithms meet subset selection criteria? *The Annals of Statistics* 870–887.
- JANSSEN, J., RADIĆ, V. and AMELI, A. (2021). Assessment of Future Risks of Seasonal Municipal Water Shortages Across North America. *Frontiers in Earth Science* 798.
- JASECHKO, S., KIRCHNER, J. W., WELKER, J. M. and McDONNELL, J. J. (2016). Substantial proportion of global streamflow less than three months old. *Nature geoscience* **9** 126–129.
- KIM, K., ŞENTÜRK, D. and LI, R. (2011). Recent history functional linear models for sparse longitudinal data. *Journal of statistical planning and inference* **141** 1554–1566.
- KIM, Y., KWON, S. and CHOI, H. (2012). Consistent model selection criteria on high dimensions. *The Journal of Machine Learning Research* **13** 1037–1057.
- KRATZERT, F., KLOTZ, D., BRENNER, C., SCHULZ, K. and HERRNEGGER, M. (2018). Rainfall–runoff modelling using Long Short-Term Memory (LSTM) networks. *Hydrology and Earth System Sciences* **22** 6005–6022.
- KUNZ, N. C. (2020). Towards a broadened view of water security in mining regions. *Water Security* **11** 100079.
- LENG, C., LIN, Y. and WAHBA, G. (2006). A note on the lasso and related procedures in model selection. *Statistica Sinica* 1273–1284.
- MACDONALD, B., RANJAN, P. and CHIPMAN, H. (2015). GPfit: An R package for fitting a Gaussian process model to deterministic simulator outputs. *Journal of Statistical Software* **64** 1–23.
- MALFAIT, N. and RAMSAY, J. O. (2003). The historical functional linear model. *Canadian Journal of Statistics* **31** 115–128.
- MEINSHAUSEN, N. and YU, B. (2009). Lasso-type recovery of sparse representations for high-dimensional data. *The annals of statistics* **37** 246–270.
- MOGES, E., RUDELL, B. L., ZHANG, L., DRISCOLL, J. M. and LARSEN, L. G. (2022). Strength and Memory of Precipitation’s Control Over Streamflow Across the Conterminous United States. *Water Resources Research* **58** e2021WR030186.
- MURARI, A., LUNGARONI, M., PELUSO, E., GAUDIO, P., LERCHE, E., GARZOTTI, L., GELFUSA, M. and CONTRIBUTORS, J. (2018). On the use of transfer entropy to investigate the time horizon of causal influences between signals. *Entropy* **20** 627.
- PESANDO, J. E. (1972). Seasonal variability in distributed lag models. *Journal of the American Statistical Association* **67** 311–312.
- RUSHWORTH, A. M., BOWMAN, A. W., BREWER, M. J. and LANGAN, S. J. (2013). Distributed lag models for hydrological data. *Biometrics* **69** 537–544.
- SATOPAA, V., ALBRECHT, J., IRWIN, D. and RAGHAVAN, B. (2011). Finding a" kneedle" in a haystack: Detecting knee points in system behavior. In *2011 31st international conference on distributed computing systems workshops* 166–171. IEEE.
- SCHUITE, J., FLIPO, N., MASSEI, N., RIVIÈRE, A. and BARATELLI, F. (2019). Improving the spectral analysis of hydrological signals to efficiently constrain watershed properties. *Water Resources Research* **55** 4043–4065.
- STAERK, C., KATERI, M. and NTZOUFRAS, I. (2018). Adaptive subspace methods for high-dimensional variable selection, PhD thesis, Universitätsbibliothek der RWTH Aachen.
- TANG, G., CLARK, M. P., PAPALEXIOU, S. M., NEWMAN, A. J., WOOD, A. W., BRUNET, D. and WHITFIELD, P. H. (2021). EMDNA: An Ensemble Meteorological Dataset for North America. *Earth System Science Data* **13** 3337–3362.
- TANNER, J. E. (1974). Variable distributed lags and forecasting non-residential construction. *Canadian Journal of Economics* 642–654.
- TIBSHIRANI, R. (1996). Regression shrinkage and selection via the lasso. *Journal of the Royal Statistical Society: Series B (Methodological)* **58** 267–288.
- TRIVEDI, P. K. and LEE, B. (1981). Seasonal variability in a distributed lag model. *The Review of Economic Studies* **48** 497–505.
- VINK, S. and ROBBINS, S. (2012). Mine water management in variable climate regimes. In *Presented at the International Mine Water Association Symposium. pp. 20A–20I*.

- WHITTAKER, E. T. (1922). On a new method of graduation. *Proceedings of the Edinburgh Mathematical Society* **41** 63–75.
- XUN, X., GUAN, T. and CAO, J. (2022). Sparse estimation of historical functional linear models with a nested group bridge approach. *Canadian Journal of Statistics*. <https://doi.org/10.1002/cjs.11747>
- YANG, L. and HONG, Y. (2017). Adaptive penalized splines for data smoothing. *Computational Statistics & Data Analysis* **108** 70–83.
- YANG, L., DING, M., HONG, Y. and WANG, X. (2021). Estimating functions and derivatives via adaptive penalized splines. *Communications in Statistics-Simulation and Computation* **50** 2054–2071.
- ZHANG, C.-H. and ZHANG, T. (2012). A general theory of concave regularization for high-dimensional sparse estimation problems. *Statistical Science* **27** 576–593.
- ZHAO, P., ROCHA, G. and YU, B. (2009). The composite absolute penalties family for grouped and hierarchical variable selection. *The Annals of Statistics* **37** 3468–3497.
- ZHAO, P. and YU, B. (2006). On model selection consistency of Lasso. *The Journal of Machine Learning Research* **7** 2541–2563.
- ZOU, H. (2006). The adaptive lasso and its oracle properties. *Journal of the American statistical association* **101** 1418–1429.